Initial Boron Uptake and Kinetics of Transient Liquid Phase Bonding in Ni-Based Superalloys

E.D. MOREAU and S.F. CORBIN

The present work details a quantitative investigation into the braze gap width dependence on the initial boron uptake (IBU) phenomena—an event which manifests during the initial stages of brazing of boron-containing filler metals. This was accomplished using *in situ* cyclic DSC of both full- and half-joint TLPB couples, *i.e.,* IN625/xBNi2/IN625 and IN625/xBNi2. All joints demonstrated a linear relationship between the isothermally solidified gap width with the square root of time which were in excellent agreement with conventional metallographic analysis methods. A conceptual model designed to quantify both the extent of isothermal solidification and IBU during TLPB in terms of the redistribution of boron as borides was implemented. The investigation demonstrated excellent agreement with microstructural and DSC results further supporting the crucial role boride formation has on the kinetics of TLPB.

I. INTRODUCTION

METALLURGICALLY, diffusion brazing (also known as transient liquid phase bonding, TLPB) generally involves the following sequential stages; melting of the filler metal, spreading and wetting of the base metal surfaces, dissolution leading widening of the initial liquid region, and the progressive isothermal solidification (IS) of the liquid phase, occasionally followed by a post-homogenization treatment.[1–8] Aside from the post-homogenization stage, the isothermal solidification (IS) stage represents the lengthiest portion of furnace brazing, typically requiring anywhere from a few hours to a day to complete; a stark contrast to the melting and gap widening (or dissolution) stages which transpire within minutes.[5,6] Many authors have attempted to quantify the process of isothermal solidification through a variety of techniques, the simplest of which involve assessing the extent of IS by metallographically measuring the thickness of any residual athermally solidified liquid as a function of brazing time.[5–12] This route is however laborious, time-consuming, and prone to experimental uncertainties, since multiple samples and extensive metallographic analysis are needed for each gap thickness and brazing time. A more efficient method, first developed by Partz and Lugscheider[13] and later employed by Arafin *et al.*[11]

and Sakamoto *et al.*,[14] consisted of placing a filler metal powder in a low-angle wedge, created from two plates of the desired base metal (BM), thereby creating a continuously varying braze gap dimension. Brazing of a series of samples at different times allows the determination of the maximum permissible clearance required to avoid the formation of athermally solidified structures per the given conditions (temperature, composition, time, *etc.*). The work ultimately provided a measure of the maximum brazing clearance (MBC), a key parameter in avoiding brittle centerline eutectic phases and achieving satisfactory TLPB. While the MBC analysis has great practical importance, it also allows interpretation of the more fundamental kinetics of TLPB, which will be utilized in the current study.

Since the isothermal solidification stage is the most significant step during TLPB, it has been extensively modeled.[3,4,8,11,14,15] A widely accepted prediction for the complete IS time, t_f in a generalized form is

$$(t_f)^{1/2} = \frac{2w_{\max}}{k},\qquad [1]$$

where $2w_{\max}$ is the starting gap width and k is a rate constant. The rate constant k is dependent on the diffusivity of the melting point depressant (MPD) element into the base metal and its concentration in the liquid and solid adjacent to the interface. In conventional TLPB, the expectation is that dissolution of the base metal occurs during initial heating, such that gap widening occurs prior to the isothermal solidification stage. In Eq. [1], dissolution is represented by $2w_{\max}$ which is generally expected to be greater than the original gap or braze insert dimensions $2w_o$. From

E. D. MOREAU and S. F. CORBIN are with the Department of Mechanical Engineering, Dalhousie University, 1360 Barrington Street, P.O. Box 15,000, Halifax, Nova Scotia, B3H 4R2, Canada. Contact e-mail: stephen.corbin@dal.ca

Eq. [1], the starting gap width present (or assumed) has a key influence over the complete IS time.

In most studies of Ni-based superalloy brazing, a linear relationship between the quantity of liquid phase remaining and the square root of time exists, which would be expected from the form of Eq. [1].[7–12] In the case of MBC curves, this translates to an increase in the isothermally solidified zone (ISZ) thickness with the square root of brazing time. Close examination of the MBC curves produced by Partz and Lugscheider,[13] Arafin et al.,[11] and Sakamoto et al.[14] work revealed that the MBC curves, when extrapolated to zero braze time, predict a non-zero ISZ width. In other words, a significant degree of diffusional solidification has occurred prior to attaining the peak brazing temperature. In other work, where a braze foil insert is place between two base metal plates, it is generally assumed that the foil insert thickness is the thickness of the original liquid or centerline eutectic at zero braze time (i.e., dissolution is assumed to be negligible).[5–12] Examination of plots of centerline eutectic width versus the square root of time from these studies reveals that the predicted initial liquid is present at zero braze time in less than the original insert thickness. This also indicates that some diffusional solidification occurs during initial heating to the braze temperature.

Ruiz-Vargas et al.[6] performed a detailed examination of the melting stages of a BNi2 foil against a pure Ni base metal. They established that boron diffusion into the base metal occurs as soon as the solidus temperature is reached. This resulted in Ni_3B precipitation and the formation of a diffusion-affected zone (DAZ). Despite some evidence of base metal dissolution during further heating, once at the peak braze temperature, a significantly developed DAZ layer and boride precipitation remained below the solid/liquid interface.

It can be concluded that, for the case of Ni-based TLPB, where boron is used as a MPD, an initial boron uptake (IBU), which reduces gap width, dominates over gap widening by dissolution. Therefore, on examining the kinetics of TLPB using the form of Eq. [1], it is important to understand the IBU process in detail, since it will determine the starting gap width at the beginning of the isothermal hold time and the IS completion time. The purpose of the current study is to examine, quantify, and explain the IBU as a function of braze gap width.

BNi2 was chosen as the braze alloy due to its wide commercial use and the fact that it contains two of the most important melting point depressants (i.e., B and Si). IN625 was chosen as the base metal also due to its wide commercial use, relatively simple microstructure as a solid solution alloy, yet containing many of the important boride formers including Cr, Mo, and Nb as outlined recently by Pouranvari et al.[16]

II. EXPERIMENTAL PROCEDURE

The 4.5-mm-diameter base metal substrates used in the current work were created via Electro Discharge Machining of a 1.9-mm-thick Inconel 625 (IN625) plate procured from McMaster Carr (ASTM B443,

AMS5599). The ≈ 48-μm-thick amorphous brazing foil or filler metal (FM), AMS 4777 (AWS BNi2) was procured from Aimtek Corporation. Discs 4.5 mm in diameter were punched from this foil. Both the IN625 and BNi2 were subject to Inductively coupled plasma-optical emission spectrometry chemical analysis, the results of which are shown in Table I. All solidification/melting studies were conducted in a Netzsch Pegasus 404 differential scanning calorimeter (DSC) under continuous flowing high-purity (99.9999 pct) argon gas at a rate of 50 mL/min, following a dual evacuation/pressurization procedure ($P = 10^{-5}$ mbar). Alumina crucibles were used in all instances as it prevented wetting and chemical interaction with the substrates or filler metal. Complete assembly of the brazing couples involved the following procedure: light grinding/polishing using 500 and 2000 grit SiC paper to obtain a smooth faying surface, ultrasonic cleaning of the FM and BM in acetone, coating of all BM surfaces, except for the faying surface(s), with a suspension of Y_2O_3 and acetone, and final assembly of the couple as illustrated in Figure 1 (left). The half-joint arrangement has the dual purpose of improving the DSC signal as described by Turriff et al.[17] and providing a light pressure between BM and FM, thereby enhancing spreading and wetting as encountered in the more practical full joint. In the current work, the possibility of expanding the DSC methodology to include the analysis of a full joint (see Figure 1 (right)) was explored. If successful, this full-joint arrangement would allow for the examination of different gap widths using the DSC method, validate the use of half-joint arrangement to study TLPB under full gap conditions, and demonstrate the ability of the DSC method to determine the maximum brazing clearance during TLPB.

A cyclic thermal profile within the DSC was implemented in most cases, which involved heating and cooling at 20 K/min between 870 °C and 1050 °C to ensure complete melting and solidification of the FM. This method allowed repeated enthalpy measurements during solidification (ΔH_t) as discussed in greater detail by other authors.[17–20] This technique enables one to examine the rate of isothermal solidification (IS) with time (above solidus) using a single specimen, thus minimizing experimental variation, while greatly reducing experimental preparation. Enthalpy measurements (ΔH_t) were expressed as a fraction of the total enthalpy of melting of the FM (ΔH_o). A liquid fraction ($L_f = \Delta H_t/(\Delta H_o)$) below unity indicates that not all the FM material placed at the joint, melted or solidified. This would be the case if diffusional or isothermal solidification has occurred.

One DSC cyclic experiment was performed for each condition, but repeat runs were performed for the IN625/2xBNi2/IN625 (full-joint) and IN625/1xBNi2 (half-joint) couples. In these repeat runs, the enthalpy measurements differed on average by 6.75 pct. Each cycle represented 15 minutes of liquid duration (or brazing time). The number of cycles completed depended on the gap thickness studied, ranging between 5 and 16 cycles representing 75 to 240 minutes of braze times.

Base Metal	Ni (min)	Fe	Co	Cr	Al	Ti	Mo	Nb	Mn	B	Si	Other
BNi2*	79.5	3.2	—	7.0	—	—	—	—	—	2.9	4.2	3.2
IN625	59.5	4.0	0.2	20.8	0.6	0.3	8.9	3.7	0.3	—	0.5	1.2

*Nominal Composition of BNi2: Ni-3.0 (2.6 at pct) Fe-7.0 (6.6 at pct) Cr-4.5 (7.8 at pct) Si-3.2 (14.5 at pct) B.
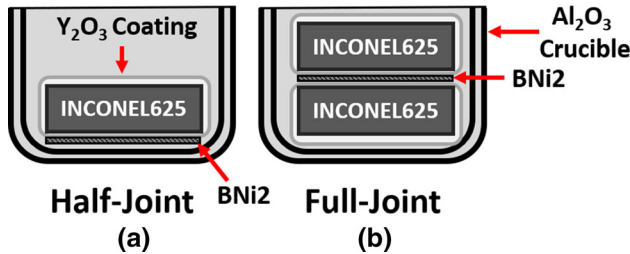

Fig. 1—Half- (*a*) and full-joint (*b*) experimental configurations. Note that in an alternate version of the depicted set-up, the faying surfaces were also coated with Y_2O_3 as described in the text.

An experimental measurement of ΔH_o is influenced by the presence of the BM arrangement within the DSC sample crucible. To determine the value of ΔH_o for each of the arrangements in Figure 1, an additional cyclic test was performed on the TLPB couples. In this case, the faying surface was coated in a thin layer of Y_2O_3 (Ni// BNi3) to prevent diffusional bonding thereby generating several, repeatable ΔH_o enthalpy measurements which were then averaged. Thus, each enthalpy measurement determined in the cyclic experiments, ΔH_t, could be expressed as a fraction of the total (100 pct) liquid present, providing a quantitative measure of the quantity of liquid present versus brazing time.

Microstructural characterization of samples after heating in the DSC involved longitudinally grinding (500 grit), followed by sequential polishing, finishing with a colloidal silica suspension. All imagings were performed in the etched condition (Kalling's waterless) using a Hitachi S4700 CFE scanning electron microscope coupled with an Oxford X-max (80 mm^2) energy dispersive spectroscopy (EDS) for chemical analysis using an acceleration voltage of 15 kV at 15 μA. Lastly, a backscatter electronic (BSE) operating mode was also used to improve the contrast between the various phases (atomic number contrast).

III. RESULTS AND DISCUSSIONS

A. DSC Analysis of Liquid Fraction

One goal of the current work was to validate whether the DSC technique described above using half joints was capable of accurately simulating isothermal solidification of an actual full joint, *e.g.*, BM/FM/BM. IN625/ 2xBNi2/IN625 (full-joint) and IN625/1xBNi2 (half-joint) TLPB couples were examined for an extended period under identical conditions. Figures 2(a) and (b) compare the melting and solidification peaks for the full and half joints for various brazing cycles and times. The cycle number (*i.e.,* 1C, 2C, etc.) and equivalent liquid duration time in minutes are indicated next to each cyclic curve.

The measurements clearly illustrate the progressive decrease in enthalpy, ΔH_t, due to IS as indicated by the shaded area under both the melting and solidification peaks. Furthermore, ΔH_t for both full- and half-joint arrangements decrease at similar rates. Additionally, the liquidus and solidus temperatures are relatively unchanged as IS progresses. As confirmed by numerous authors,[12,13,18] the dual melting and solidification peaks observed are associated with the ternary and binary melting/solidification events involving γ-(Ni), Ni_3B, and β-Ni_3Si. A small third peak, which occurs at the lowest temperature and only present during the initial heating (point A), is believed to pertain to a minor quantity of Chromium-rich borides formed during delayed recrystallization from the amorphous FM.[6,13]

The repeated enthalpy measurements ΔH_t can be related to liquid fraction L_f, provided there is a means of assessing the progress of IS. This involves creating an additional specimen identical to that under investigation, however, with the faying surface coated with Y_2O_3 as described in the methodology. For comparison purposes, the enthalpy of fusion ΔH_o for the BNi2 foil alone was measured as 220 J/g. The same foil melted in the presence of a fully coated (Y_2O_3).

BM in the half- and full-joint arrangements depicted in Figure 1 had half-joint enthalpies (ΔH_{oh}) of 218 J/g and full-joint enthalpies (ΔH_{of}) 132 j/g, respectively. This reduced enthalpy in the presence of the BM is due to a thermal dampening effect as first described by Kuntz *et al.*[20]

Using the above ΔH_{oh} and ΔH_{of} values, the liquid fraction L_f data versus time (min$^{1/2}$) was determined for the half joint using a single BNi2 foil and full joints using 1×, 2×, and 3× BNi2 foils. The results are plotted in Figure 3, which demonstrate a linear relationship ($R^2 > 0.95$) between L_f and $t^{1/2}$ such that linear regression can be applied to obtain the following equation:

$$\frac{H_t}{H_{oh}} = L_f = -k_L\sqrt{t} + L_o, \qquad [2]$$

where ΔH_t and ΔH_{oh} (or ΔH_{of}) have their previously defined meanings in {J/g}, L_f is the corresponding liquid fraction remaining at time t, $-k_L$ is the solidification rate {fraction/min$^{-1/2}$}, and L_o is the initial liquid fraction present at $t = 0$. The time for complete IS, t_f, can be expressed from Eq. [2] when $L_f = 0$, or
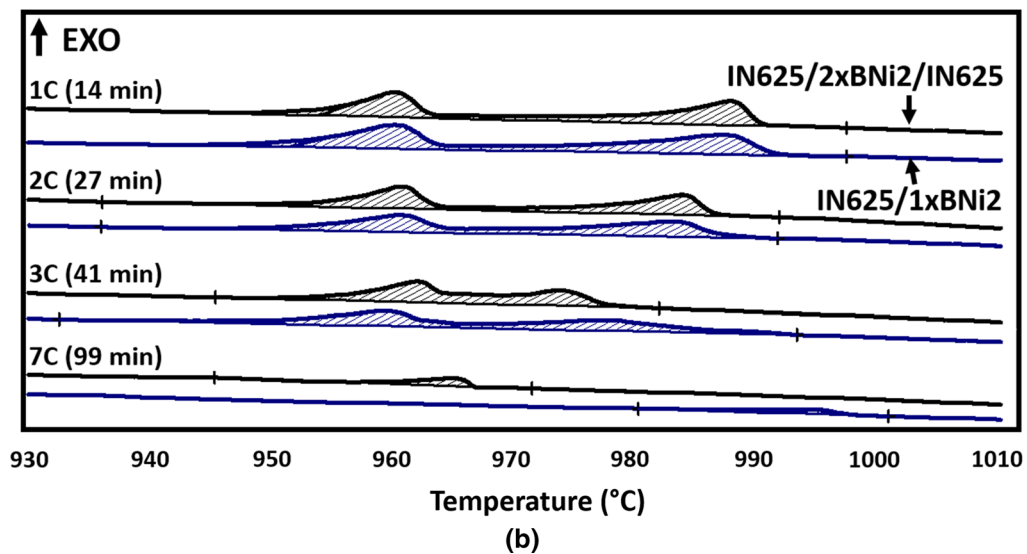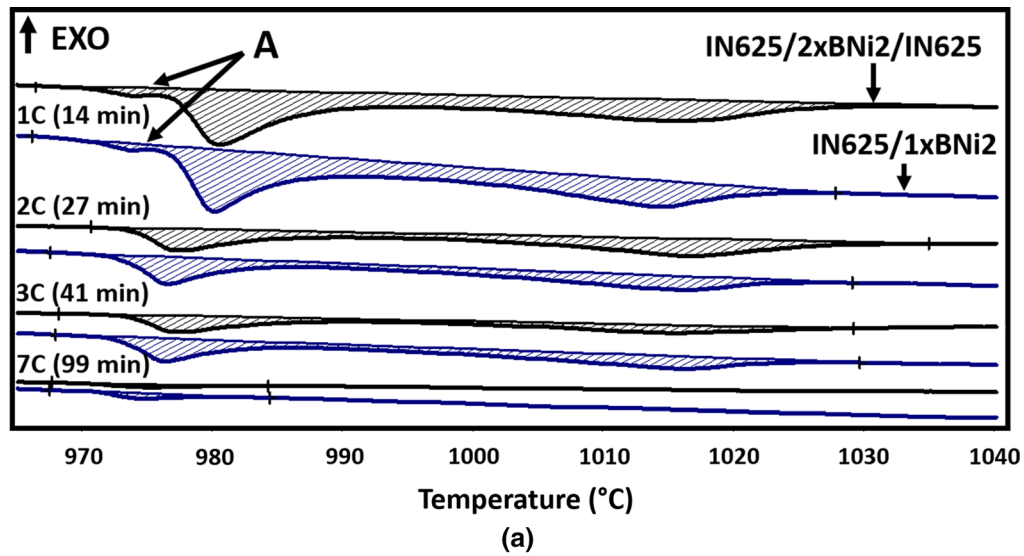
Fig. 2—Cyclic DSC melting (*a*) and solidification (*b*) measurements for IN625/2xBNi2/IN625 (full joint) and IN625/1xBNi2 (half-joint) TLPB couples.

$$t_f = \left(\frac{L_o}{k_L}\right)^2 \qquad [3]$$

Figure 3 indicates that as the number of BNi2 foils decrease, L_o and t_f decrease, which corresponds to a decreasing gap width, $2w_o$. The data for the 1 × foil ½-joint and the 2 × full joint are similar, resulting in a similar value for t_f. This confirms that DSC analysis of the ½ joint arrangement can correctly represent a full-joint geometry with an equivalent gap width.

As pointed out by Murray and Corbin,[18] the L_f measurements from the DSC can be converted to the width of liquid phase remaining in the gap $2w_t$ {μm}, provided that the original thickness of the braze gap $2w_o$ is known:

$$2w_t = \frac{H_t}{H_o}2w_o = L_f 2w_o \qquad [4]$$

Combining Eqs. [1] and [3]

$$2w_t = 2w_o\left(-k_L\sqrt{t} + L_o\right) = -k_w\sqrt{t} + 2w_i, \qquad [5]$$

where $k_w = 2w_o k_L$ {μm/min$^{1/2}$} and $2w_i = 2w_o L_o$ {μm}.

For each sample, a value of w_o was obtained from multiple measurements of FM thickness made on post-braze polished cross sections of the DSC samples. Using these measurements, the liquid fraction data of Figure 3 are replotted as liquid width remaining, in Figure 4.

The plot shows that repeated enthalpy measurements made using the DSC can provide a measure of the degree of IS in terms of the thickness of the remaining
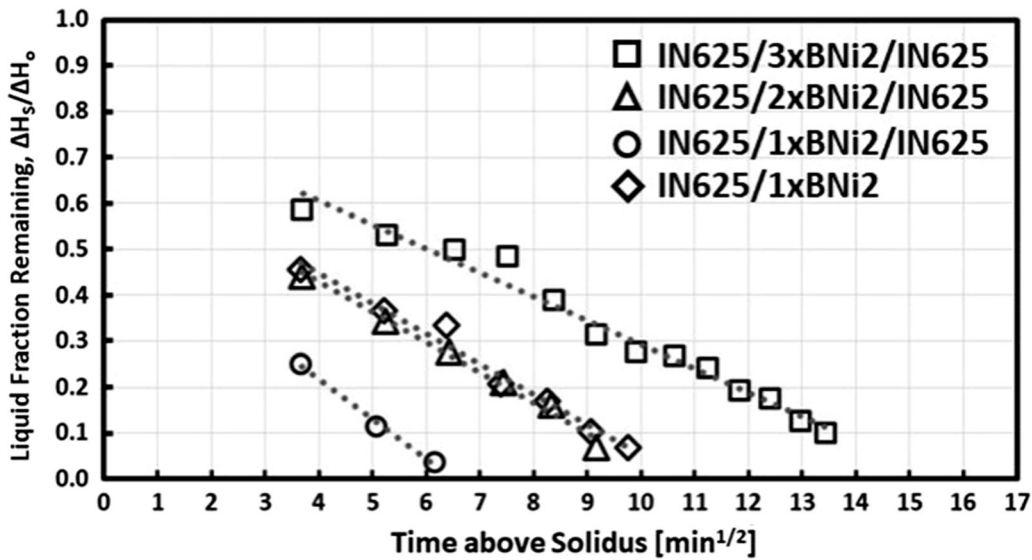
Fig. 3—Liquid fraction remaining ($\Delta H_t/\Delta H_o$) as a function of brazing time (min$^{1/2}$) for 2xIN625-1xBNi2, 2xIN625-2xBNi2, 2xIN625-3xBNi2 full joints and 1xIN625-1xBNi2 half joint.
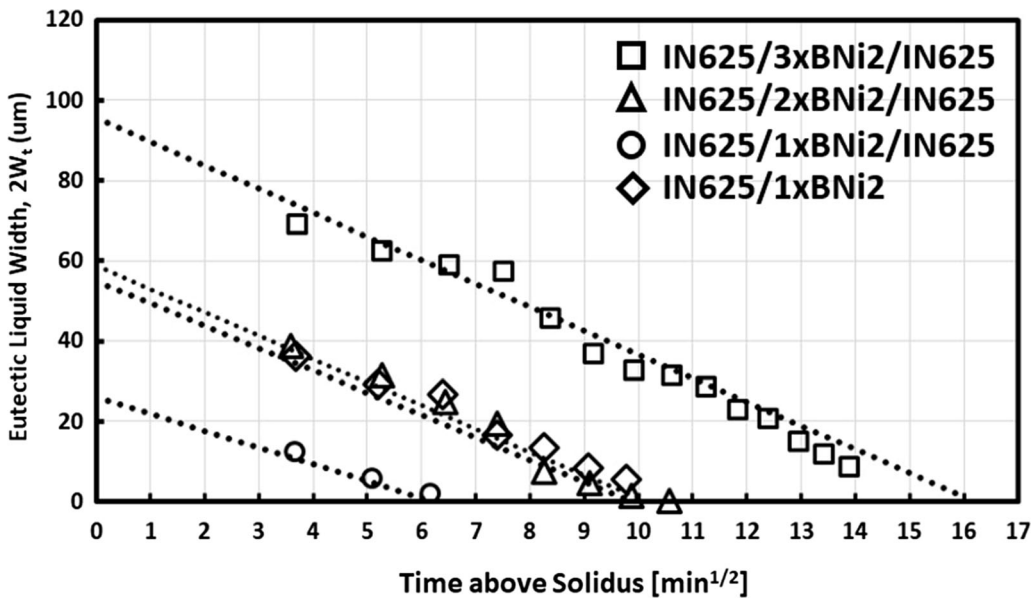

Fig. 4—Corresponding width of eutectic liquid remaining ($2W_t$) as a function of brazing time (min$^{1/2}$) for 2xIN625-1xBNi2, 2xIN625-2xBNi2, 2xIN625-3xBNi2 full joints and 1xIN625-1xBNi2 half joint.

liquid phase. This thickness can be validated by measuring the width of athermally solidified eutectic, as described in the section below.

B. Microstructural Validation of DSC Isothermal Solidification Analysis

To validate the DSC results, an additional IN625/1xBNi2 half joint was heated to the brazing temperature (1050 °C) and immediately furnace quenched (approx. 50 °C/min). Figure 5(a) illustrates the polished cross section of this sample which experienced a liquid duration brazing time of 8 minutes. For comparison, Figure 5(b) presents the microstructure of the half-joint

configuration corresponding to the DSC data from Figures 2 and 3 which exhibited a liquid duration of 96 minutes (1.6 hours). Figure 5(a) illustrates the 3 regions typical of a TLPB Ni-based superalloy joint; an isothermally solidified zone (ISZ), the diffusionally affected zone (DAZ), and the athermally solidified zone (ASZ). With an 8-minute braze time, the joint has a significant liquid fraction (ASZ) present, as expected. With the longer braze time, the sample of Figure 5(b) exhibits nearly complete IS, with only a small layer of ASZ at the top of the joint. This is consistent with the DSC data which indicate that this sample had a liquid fraction, L_t = 0.07 (7 pct) at the end of the braze time (see the IN625/1xBNi2 data set of Figure 3).
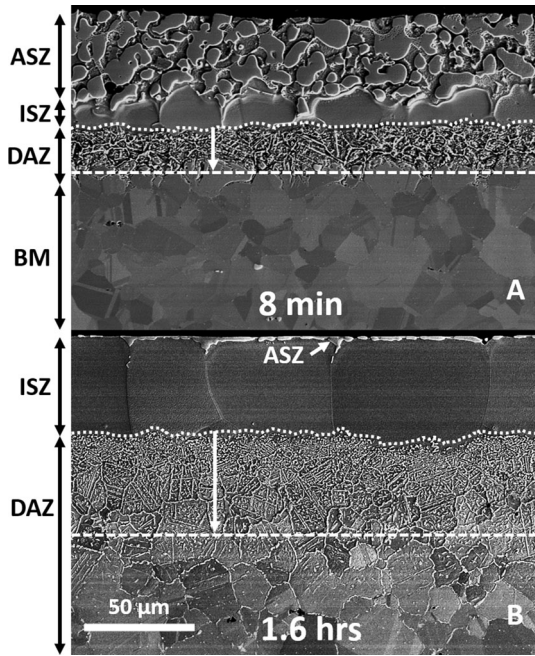
Fig. 5—Microstructure of the interrupted (*a*) and cycled (*b*) 1xIN625/1xBNi2 half-joint specimens. The meaning of the white arrows will be discussed in Section IV.

Fig. 6—Schematic illustrating the influence that initial gap width has on the liquid width of a joint during brazing. (*a*) Small gap width, (*b*) large gap width.

C. *Rate of IS and the Maximum Brazing Clearance (MBC)*

Determining the liquid width, either through DSC analysis or from post-brazing centerline eutectic metallography, has been the primary way to measure the kinetics of IS during TLPB.[5–12] One limitation of this approach is that the liquid width (or centerline eutectic width) values depend on the initial gap width, as demonstrated by the full-joint analysis of Figures 3 and 4. The basic kinetics of IS should only be dependent on the compositions of the filler and BM and the brazing temperature. This can be further explained by Figure 6 below.

The schematics A and B in Figure 6 depict two braze joints of different initial gap widths ($2w_{o1} < 2w_{o2}$). Both joints are assumed to have experienced the same braze temperature and time, such that a small amount of isothermal solidification has occurred. The liquid widths $2w_{t1}$ and $2w_{t2}$ are different since the initial gap widths are different. However, since the growth of the ISZ and DAZ regions is dependent only on the rate of diffusion and not the initial gap width, their thickness should be identical for both joints (*i.e.*, $2w_{ISZ1} = 2w_{ISZ2}$ and $2w_{DAZ1} = 2w_{DAZ2}$). In other words, the following relations hold

$$2w_{ISZ1} = 2w_{ISZ2} = (2w_{o1} - 2w_{t1}) = (2w_{o2} - 2w_{t2}) \quad [6]$$

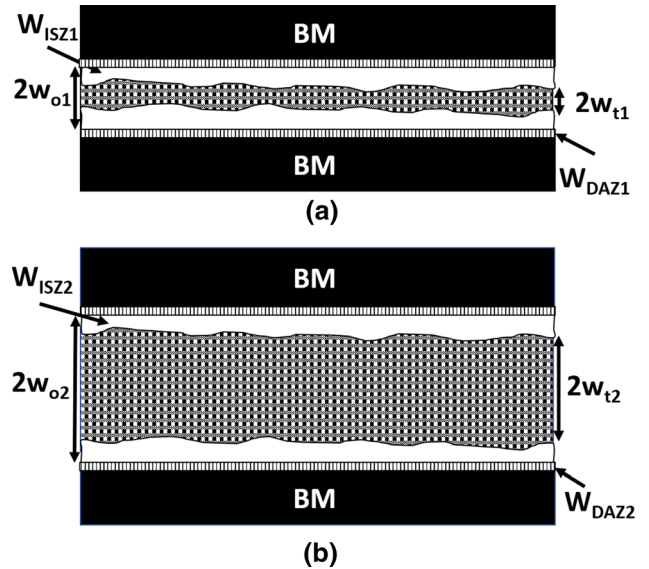Further, if both sides of Eq. [6] are divided by $2w_{o1}$ or $2w_{o2}$ we get

$$(2w_{ISZ1}/2w_{o1}) = (2w_{o1} - 2w_{t1})/2w_{o1} \text{ or } (2w_{ISZ2}/2w_{o2})$$
$$= (2w_{o2} - 2w_{t2})/2w_{o2}$$

$$[7]$$

Recognizing that $L_f = 2w_t/2w_o$ Eq. [6] can be rearranged to

$$2w_{ISZ} = 2w_o(1 - L_f) \quad [8]$$

As described in Eq. [2], the DSC measurements can determine L_f as a function of braze time. Using Eq. [8] the thickness of the ISZ layer as a function of braze time can be determined, provided the initial gap width $2w_o$ is measured from post-brazing metallographic analysis.

Metallographic measurements of $2w_o$ for the 1xBNi2, 2xBNi2, 3xBNi2 full joints and 1xBNi2 ½ joint were 43, 89, 118, and 84 μm, respectively. Using these values and the L_f data of Figure 3, the ISZ thickness $2w_{ISZ}$ for all four samples is plotted versus the square root of time in Figure 7. A consequence of plotting the data in this way is that the rate of growth of the ISZ layer is more easily seen to be the same for all samples, and independent of gap width, as proposed above. The influence of gap width is only through the time of isothermal solidification, which increases as the gap width increases. This form of plot is also more useful in allowing the prediction of the isothermal solidification time, $t_x^{1/2}$ for any gap width, or MBC_x (or $2W_{ISZ,i}$) of interest, as noted in Figure 7.

The data also point out that, regardless of gap width, all joints exhibit a similar y-intercept value at zero brazing time. Linear regression analysis of the data of Figure 7 allows a determination of this value, $2w_{ISZo}$

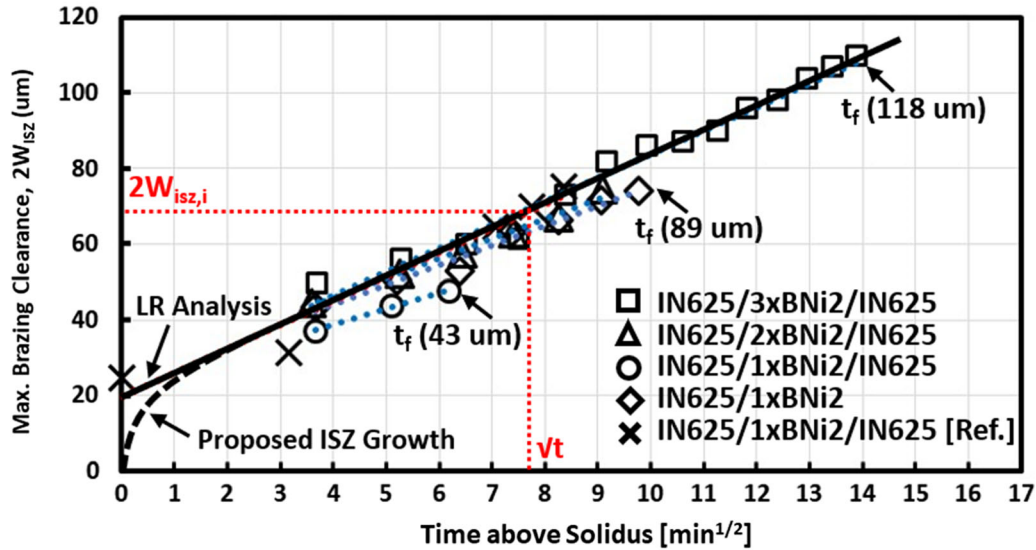$$2w_{ISZ} = k_w t^{1/2} + 2w_{ISZo}, \quad [9]$$

Fig. 7—Maximum brazing clearance ($2W_{ISZ}$) as a function of brazing time ($\text{min}^{1/2}$) for 2xIN625-1xBNi2, 2xIN625-2xBNi2, 2xIN625-3xBNi2 full joints and 1xIN625-1xBNi2 half joint. X data are taken from Reference [11].

Table II. Results of Linear Regression from Isothermal Solidification Data

Sample	k_L ($\text{min}^{-1/2}$)	L_o	$2w_{ISZo}$ (μm)	$-k_w$ ($\mu m/\text{min}^{1/2}$)	$2w_o$ (um)
1xIN625/1xBNi2	-0.07	0.69	22.99	5.25	84 ± 4
2xIN625/1xBNi2	-0.09	0.56	21.62	4.27	43 ± 4
2xIN625/2xBNi2	-0.07	0.71	20.58	6.10	89 ± 18
2xIN625/3xBNi2	-0.05	0.81	21.46	6.23	118 ± 5

Arafin et al.[11]: $-k_w = 6.35$, $2w_{ISZo} = 19.61$ um.

where the rate constant k_w has the same value as before, but $2w_{ISZo}$ is the isothermally solidified width obtained by extrapolating $2w_{ISZ}$ to zero time (i.e., the Y-intercept). Table II lists the values from linear regression obtained from both Eqs. [2] and [9]. The value of $2w_{ISZo}$ is very close for all full and half joints studied. It also agrees very closely to data that can be derived from a wedge gap/metallography-type analysis previously performed by Arafin et al. on IN625/BNi2 brazed joints at 1050 °C.[11]

The value of $2w_{ISZo}$ (i.e., ~ 21 μm in the current case) is convenient mathematically but lacks physical meaning. As shown by Ruiz-Vargas et al.[6] and Murray and Corbin,[18] no boron diffusion or ISZ formation occurs prior to reaching the solidus temperature of the filler metal (i.e., zero braze time). Furthermore, rapid growth of the ISZ has been observed during initial heating between the solidus and peak braze temperature [6,7]). Consequently, it is proposed that the ISZ rapidly grows while heating from the solidus to the braze temperature as a metallurgical interface is first formed between the BM and filler metal (see Figure 7). Once the braze temperature is reached, the rate of ISZ growth follows the isothermal linear regression rate. Therefore, a more physically meaningful value for the initial ISZ width is $2w_{ISZi}$, which can be determined from Eq. [9] using the time taken to heat from the solidus to the braze temperature, (i.e., $t = 4.3$ minutes, resulting in a $2w_{ISZi}$ ~ 33 μm).

The impact of the presence of an IBU in interpreting TLPB kinetics can be demonstrated through the use of Eq. [1]. The value of k can be determined using the isothermal solidification time measured for the 3 full gaps of this study (i.e., 6.25, 10.1, and 16 (min)$^{1/2}$) for the $2w_o$ gaps of 43, 89, and 118 μm, respectively). The average k value assuming the starting gap width of $2w_o$ for these three samples was 7.80 $\mu m/\text{min}^{1/2}$. Alternatively, if the IBU formation is taken into account, the actual starting gap width is $2w_t = 2w_o - 2w_{isz}$. Using the values of $2w_{isz}$ from Table II results in $2w_t$ of 27.4, 62.4, and 96.5 μm for the increasing gap widths and an average k of 5.53 $\mu m/\text{min}^{1/2}$ when taking into account the IBU. From the work of Murray and Corbin,[18] $k = 4\text{erf}^{-1}(C_s/C_o)D^{1/2}$ where C_s and C_o are the boron composition in the solid adjacent to the solid–liquid interface and in the filler metal, respectively, and D is the diffusivity of boron in the base metal at 1050 °C. Using 0.3 and 13.7 at pct for C_s and C_o along with the k values determined above for neglecting, and considering an IBU, results in diffusivity values of 1.7×10^{-10} and 8.5×10^{-11} m^2/s, respectively. Both these values for diffusivity are within the range reported by other

researchers. However, it is expected that the value of 8.5×10^{-11} m^2/s is a more accurate description for kinetics in this system since it uses a starting gap width that accounts for the IBU.

The microstructures of the completely solidified full joints (*e.g.*, 1xBNi2, 2xBNi2 and 3xBNi2) used to acquire the IS data are displayed in Figure 8. All three specimens consist of an ISZ which increases in width as the number of BNi2 foil layers increases. The ISZ consists of large grains of solid solution of γ-(Ni). These grains grew epitaxially from each solid–liquid interface, meeting in the middle when all the liquid was removed. All samples also have a DAZ due to the diffusion of Boron from the liquid (BNi2) into the BM (IN625) forming Chromium-rich Borides (with Mo, Nb in minor concentrations). The thickness of the DAZ increases with increasing MBC. This is partly due to the longer brazing times required to cause complete IS with an
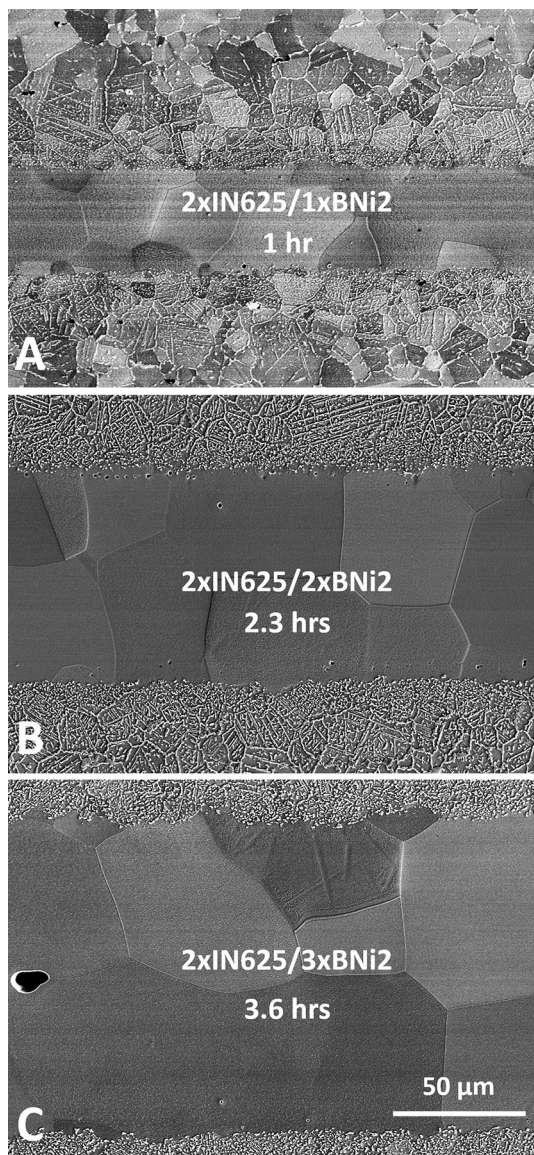
increase in MBC. There is also an increased quantity of boron within the MBC that must be removed during TLP brazing.

Further evaluation of the progress of IS as a function of both time and gap width was performed by comparing the severity of the DAZ as shown in Figure 9. As the gap width increases, the time needed for complete IS increases and this results in a thicker DAZ region. At the leading edge of the DAZ, the borides form along the grain boundaries. Over time, the grains covered by the borides begin to form discrete boride particles followed by continuous needle-shaped borides. This progression of boride distribution from 1 to 3.6 hours indicates that boron diffuses first by grain boundary diffusion, followed by diffusion within the grains.

D. *Conceptual Model for IBU Formation and IS Rate in Terms of Boride Formation*

An explanation for the development of the IBU can be given with reference to the conceptual model of Figure 10. Prior to reaching the solidus temperature, the interface consists of the FM with a boron concentration C_o and a base metal with a boron concentration of C_m. Once the solidus is exceeded some liquid forms, greatly accelerating mass transport. This allows the establishment of the required phase equilibria at the process temperature between the BM and FM. Analysis of a simpler Ni-Si-B ternary braze system has shown that diffusion path theory determines the phase equilibria and structure at the interface.[21] In Ni-B-based systems, this structure consists of an ISZ layer with a very low boron concentration C'_m and a DAZ containing a high boron concentration in the form of precipitated borides. With reference to Figure 10, the formation of this interface involves a transformation of a small volume element, $A_o \Delta w_{DAZ}$ from BM to DAZ. Similarly, it requires the transformation of a small volume element $A_o \Delta w_{FM}$ (or $A_o \Delta w_{ISZ}$) from FM to ISZ. If it is assumed that the concentration of boron in the BM and ISZ is

Fig. 8—SEM micrographs of all full-joint specimens (*a*) 1 h, (*b*) 2.3 h, (*c*) 3.6 h.
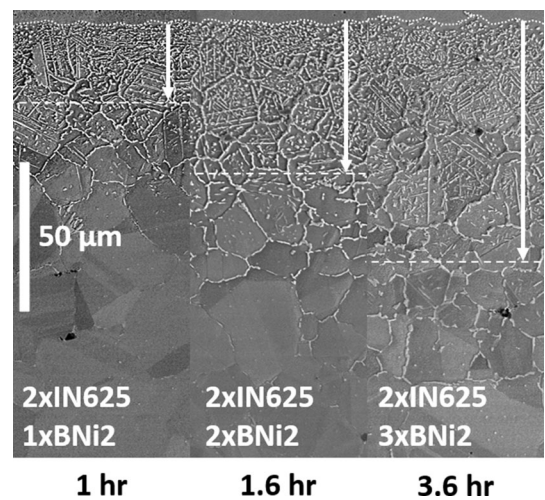

Fig. 9—DAZ of full joints upon achieving complete isothermal solidification. The meaning of the white arrows will be discussed in Section IV.
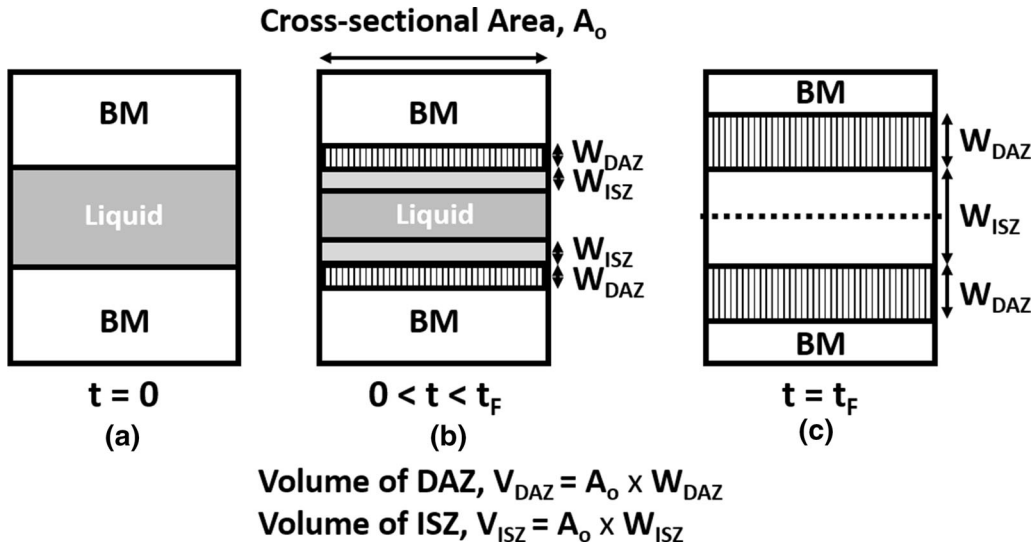
Cross-sectional Area, A_o

Fig. 10—Schematic representing redistribution of Boron from the liquid phase to borides in DAZ during TLPB, (a) time zero ($t = 0$), (b) intermediate time between zero and final ($0 < t < t_f$), (c) at complete isothermal solidification time ($t = t_f$).

negligible (*i.e.*, $C_m = C'_m = 0$), then the amount of boron that was contained in the small volume of FM must be redistributed to the DAZ layer. The quantity of Boron contained within the FM is known and can be expressed as

$$m_{BFM} = V_{FM}C_o, \qquad [10]$$

where m_{BFM} is the mass of FM, C_o is the volume concentration of boron in the filler in g/cm^3, and V_{FM} is the volume of filler in the joint that has undergone isothermal solidification.

The boron content within the DAZ is based on the volume fraction of borides and their concentration within the BM matrix. Solubility values for B in γ-Ni at 1050 °C of 0.05 wt pct B and 0.073 wt pct were obtained using Thermocalc Thermodynamic modeling software for IN625 and Ni-7Cr-3Fe-4.5Si (*i.e.*, the ISZ), respectively. Since these values are very low, the boron contents in the IN625 matrix within the DAZ and ISZ were neglected, as mentioned above. The mass of boron in the DAZ m_{BDAZ} can then be expressed as

$$m_{BDAZ} = V_{DAZ}X_{DAZ}f_i\rho_i, \qquad [11]$$

where X_{DAZ} is the volume fraction of borides present within the DAZ layer, V_{DAZ} is the volume of the DAZ layer, f_i is the weight fraction of boron in the principal boride intermetallic, and ρ_i is the specific gravity {g/cm^3} of the precipitate (boride) phase, *i*. Under the assumption that the mass of boron removed from the FM as it undergoes IS is redistributed to the growing DAZ (*i.e.*, $m_{BFM} = m_{BDAZ}$) Eqs. [10] and [11] combined to become

$$V_{DAZ}X_{DAZ}f_i\rho_i = V_{FM}C_o \qquad [12]$$

From Figure 10, $V_{DAZ} = A_o\Delta w_{DAZ}$ and $V_{FM} = V_{ISZ} = A_o\Delta w_{ISZ}$ allowing the above equation to reduce to

$$w_{DAZ}X_{DAZ}f_i\rho_i = w_{ISZ}C_o. \qquad [13]$$

The value of Δw_{ISZ} in Eq. [13] is the amount of FM that has undergone isothermal solidification, which can be determined as a function of braze time from the DSC analysis, using Eq. [9]. A final rearrangement of Eq. [13] gives

$$w_{DAZ} = \frac{w_{ISZ}C_o}{X_{DAZ}f_i\rho_i}. \qquad [14]$$

The fraction of borides within the DAZ, X_{DAZ} was determined experimentally using image analysis applied to the polish cross sections of Figures 5(a) and 9. A 600-time magnification was used and the width of the image analyzed was 210 μm. For the short hold sample of Figure 5(a), the thickness of the individual elements analyzed was 2 μm in order to get enough depth resolution. For the samples of Figure 9, an element thickness of 3.3 μm was used. The data for these four samples are plotted as a function of depth within the DAZ layer in Figure 11. It was assumed that the distribution of borides within the DAZ was isotropic such that the volume fraction was equivalent to the measured area fraction. Due to the slightly uneven ISZ/DAZ interface, reliable area fractions within the first 2 μm of depth were not possible. For positions of zero and 2 μm depth, it was assumed that the area fraction of borides was the same as that measured at a depth of 3.3 or 4 μm.

From Figure 11 the area fraction is highest near the ISZ/DAZ interface, varying in the range of 27 to 33 vol pct. This maximum value is consistent for all braze joints regardless of the braze time or the gap width used. It highlights that there is a dense band of precipitates (DBP) that forms adjacent to the ISZ/DAZ interface. In this DBP, borides have formed along the grain
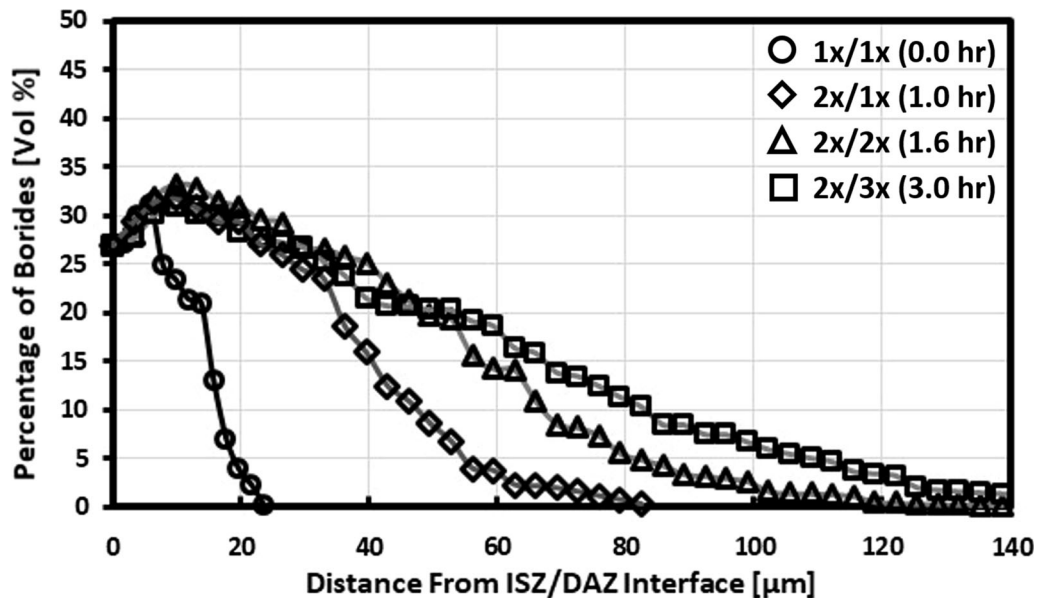
Fig. 11—Experimentally determined volume percent of borides as a function of depth into the DAZ.

boundary and within the grain interior. The microstructure transitions to borides covering the grain boundary with only isolated borides in the grain, corresponding to a drop in the boride volume below 20 vol pct. Eventually, borides are only present at grain boundaries and their volume percent drops below 5 pct.

The data of Figure 11 and image of Figure 5(a) show that during the initial stages of brazing, which closely corresponds to the observed IBU formation, the DAZ consists primarily of a DBP layer. In the full joints cycled to complete IS, this region grows to a thickness of approximately 40-45 μm. The primary influence of gap size and longer braze times is in the growth of the DAZ regions containing boride volume fractions below 20 pct. Using data from all four samples depicted in Figure 11, the average area percent of borides within the DBP region was determined to be 28 pct.

The values of f_i and ρ_i in Eqs. [11] through [13] depend on the type of boride formed within the DAZ. A detailed characterization study performed by Zhang et al.[22] indicated that M_3B_2 and M_5B_3 were the dominant boride phases formed in a Ni-based superalloy MAR-M247, which contained W. These boride stoichiometries also appeared to be prevalent in other works where the base metals contained W, as summarized in a review published by Pouranvari et al.[16] Recent work by Bai et al.[23] used a novel XRD methodology which identified the predominant formation of MB-type borides, while MB_2, M_5B_3, and M_3B_2 were also detected, in the W-free IN718 alloy. They also performed thermodynamic modeling using Thermocalc which confirmed the prevalence of MB borides in the DAZ of IN718. Since the alloy IN625 of this study is also W free and has the same boride former elements as IN718 (i.e., Cr, Mo, Nb), it is expected that the predominant borides present in the DAZ should also be similar to IN718. Quantitative EDS analysis was used to confirm this expectation.

The Oxford X-max (80 mm^2) used in the current study is equipped with a windowless EDS detector, which allows the detection of boron. Using the low voltage condition of 5 kV outlined in Reference 24 for quantitative boron measurements in superalloys, accurate boron concentrations in the DAZ borides were obtained. BSE imaging identified light contrast borides with a pct composition of 64 B, 16 Cr, 14.6 Mo, 2.3 Nb, 2.7 Ni, and 0.4 Fe and dark contrast borides with a pct composition of 59 B, 36 Cr, 2.7 Mo, 0.1 Nb, 2.0 Ni, and 0.2 Fe. The light-contrasted borides represented approximately 95 pct of the total borides. On the basis of these measurements, it was concluded that the boride types in the DAZ are of the MB and MB_2 stoichiometry

With the type of boride selected, a $f_i = 0.211$ was used for the boron weight fraction in the borides. The densities reported for the most commonly encountered binary Cr-rich borides do not consider the presence of other common boride formers such as Mo, Nb, W, etc., which are commonly detected in boride precipitates.[22,23,25,26] Their influence is likely a minor increase in the overall density of a particular boride, given their greater molecular mass and mutual solubility, e.g., M = Cr, Mo, W, etc. Considering the prominent MB stoichiometry expected in the current alloy within the DAZ, a ρ_i of 6.202 g/cm^3 was selected.

The thickness of the isothermally solidified layer formed during initial heating was determined from the DSC data to be $2w_{ISZi} \sim 33$ μm. The volume concentration of boron in the BNi2 filler, $C_o = 0.247$ g/cm^3. It is assumed that the DAZ at the IBU stage can be represented by the arithmetic mean of the X_{DAZ} data in Figure 11 (i.e., 0.178) and f_i and ρ_i have the values determined above. Using these values, Eq. [14] predicts a DAZ thickness $2w_{DAZ}$ of 35.0 μm or w_{DAZ} on a half-joint basis of 17.5 μm. The white arrow in Figure 5(a) represents this prediction, which agrees well with the actual depth of the DAZ observed.

The mass balance equation of Eq. [13] is also applicable to the complete IS cycles depicted in Figures 5(b) and 9. These full cycle samples are composed of the DBP and the lower volume fraction boride precipitate region. In these cases, an average boride fraction was determined as 16.5, 15.3, and 14.0 for the $2x/1x$, $2x/2x$, and $2x/3x$ joints, respectively, and 15.3 for the $1x/1x$ half joint of Figure 5(b). The values of $2w_{ISZ}$ upon complete IS would be equal to the $2w_o$ values given in Table II. Using the same values of C_o, f_i and ρ_i as above, Eq. [13] predicts the average half-joint w_{DAZ} to be 22.8, 47.2, and 62.5 μm for the three increasing joint gaps and 47.2 for the half joint. As indicated by the white arrows in Figures 5(b) and 9, these predictions are smaller than the full depth of the experimental DAZ width. This is due to the use of the average X_{DAZ} values used in Eq. [14]. Therefore, the predictions represent the DAZ depth expected if the boride fractions were uniformly distributed at the average X_{DAZ} values of 16.5, 15.3, and 14.0.

IV. CONCLUSIONS

The principal findings acquired in the present study have been summarized below:

1. Validated the use of IN625/BNi2 half-joint DSC configuration for quantitatively simulating TLPB behavior of IN625/2xBNi2/IN625 full-joint couples, which showed a strong agreement with prior literature reports using metallography-based analysis.
2. Successful extension of the analysis to determine the MBC curve for a given BM/FM and braze temperature from a single cyclic DSC experiment.
3. Solidification exhibited solid-state diffusion process governed by the diffusion of B from the liquid to the BM, forming Cr-rich (Mo, Nb) borides in the DAZ. Thus, the rate of IS was independent of the thickness of the gap, whereas the total solidification time depended on the total quantity of Boron present. Consequently, the width of the DAZ is also proportional to the total Boron content and starting gap width.
4. Significant diffusional solidification occurs during initial heating/melting (IBU) such that approx. 20 μm of epitaxial growth of the ISZ develops prior to attaining the max. temperature (1050 °C) as confirmed by both DSC and microstructural observations.
5. The conceptual model explored herein showed that the TLPB behavior of Ni-based superalloys using Boron-containing filler metals is not only dependent on the distribution of the borides, but also the type, i.e., M_xB. The type of boride is largely determined by the base metal composition indicating that certain BM's may be more amenable to TLPB based on their boride forming characteristics.

REFERENCES

1. W.D. Macdonald and T.W. Eagar: *Annu. Rev. Mater. Sci.*, 1992, vol. 22, pp. 23–46.
2. D.S. Duvall, W.A. Owczarski, and D.F. Paulonis: *Weld. J.*, 1974, vol. 53 (4), pp. 203–14.
3. I. Tuah-Poku, M. Dollar, and T.B. Massalski: *Metall. Trans. A.*, 1988, vol. 19A (3), pp. 675–86.
4. H. Nakagawa, C.H. Lee, and T.H. North: *Metall. Trans. A.*, 1991, vol. 22A, pp. 543–55.
5. G.O. Cook and C.D. Sorensen: *J. Mater. Sci.*, 2011, vol. 46, pp. 5305–23.
6. J. Ruiz-Vargas, N. Siredey-Schwaller, P. Bocher, and A. Hazotte: *J. Mater. Proc. Tech.*, 2013, vol. 213, pp. 2074–80.
7. M. Pouranvari, A. Ekrami, and A.H. Kobabi: *Weld. J.*, 2014, vol. 93, pp. 60s–68s.
8. M. Pouranvari, A. Ekrami, and A.H. Kobabi: *Can. Met. Q.*, 2014, vol. 53, pp. 38–46.
9. K. Tokoro, N.P. Wikstrom, O.A. Ojo, and M.C. Chaturvedi: *Mat. Sci. Eng. A.*, 2008, vol. 477A, pp. 311–18.
10. S. Omori, Y. Hashimoto, K. Shoji, K. Hidaka, Y. Kohira, and F. Oyobi: *Funmatsuyakin*, 1972, vol. 18, p. 316.
11. MA Arafin, M Medraj, DP Turner, and P Bocher: *Mater. Sci. Eng. A*, 2007, vol. 447, pp. 125–33.
12. S.K. Tung, L.C. Lim, and M.O. Lai: *Scr. Mater.*, 1996, vol. 34, pp. 763–69.
13. K.D. Partz and E. Lugscheider: *Weld. J.*, 1983, vol. 62, pp. S160–S164.
14. A. Sakamoto, C. Fujimara, T. Hattori, and S. Sakai: *Weld. J.*, 1989, vol. 68, pp. 63–67.
15. Y Zhou, WF Gale, and TH North: *Int. Mater. Rev.*, 1995, vol. 40, pp. 181–96.
16. M Pouranvari, A Ekrami, and A Kokabi: *J. Sci. Technol. Weld. Join.*, 2018, vol. 23, pp. 13–18.
17. S.F. Corbin, S. Winkler, D.M. Turriff, and M. Kozdras: *Metall. Mater. Trans. A*, 2014, vol. 45A, pp. 3907–15.
18. D.C. Murray and S.F. Corbin: *J. Mater. Proc. Tech.*, 2017, vol. 248, pp. 92–102.
19. M.L. Kuntz, Y. Zhou, and S.F. Corbin: *Metall. Mater. Trans. A.*, 2006, vol. 37A, pp. 2493–2504.
20. M.L. Kuntz, S.F. Corbin, and Y. Zhou: *Acta Mater.*, 2005, vol. 53, pp. 3071–82.
21. E. Moreau and S.F. Corbin: *Metall. Mater. Trans. A*, 2019, vol. 50A, pp. 5678–88.
22. B. Zhang, G. Sheng, Y. Jiao, Z. Gao, X. Gong, H. Fan, and J. Zhong: *J. Alloys Compds.*, 2017, vol. 695, pp. 3202–10.
23. K. Bai, F.L. Ng, T.L. Tan, T. Li, and D. Pan: *J. Alloys Compds.*, 2017, vol. 699, pp. 1084–94.
24. J. Berlin: *Imaging Microsc. (EMS)*, 2011, vol. 13, pp. 19–21.
25. A.G. Kvashnin, A.R. Oganov, A.I. Samtsevich, and Z. Allahyari: *J. Phys. Chem. Lett.*, 2017, vol. 8, pp. 755–64.
26. A. Schnell, A. Stankowski, E. deMarcos, Proc. GT2006 ASME Turbo 2006: Power for Land, Sea, and Air. 2006, pp. 949–61.